Radiation Damage Assessment of Atomically Thin Membranes

by

Sean M. Parks

Submitted to the
Department of Mechanical Engineering
in Partial Fulfillment of the Requirements for the Degree of

Bachelor of Science in Mechanical Engineering and Physics

at the

Massachusetts Institute of Technology

February 2020

Signature of Author: Signature redacted
Department of Mechanical Engineering
January 17, 2020

Certified by: Signature redacted
Rohit Karnik
Professor of Mechanical Engineering
Thesis Supervisor

Signature redacted

Accepted by: _____
Maria Yang
Professor of Mechanical Engineering
Undergraduate Officer

Radiation Damage Assessment of Atomically Thin Membranes

by

Sean M. Parks

Submitted to the Department of Mechanical Engineering
on January 17, 2020 in Partial Fulfillment of the
Requirements for the Degree of

Bachelor of Science in Mechanical Engineering and Physics

ABSTRACT

This thesis investigates the methodologies and results of gas transport across atomically thin membranes, which are relevant to reducing Tritium inventory in fusion reactors by separating Helium from the plasma exhaust stream. A novel experimental apparatus and set-up is devised to measure the gas transport rate across a membrane by containing a pool of liquid water that evaporates over time and passes through the membrane interface to the environment. This device minimizes flow resistance on both sides, allowing for membrane resistance changes to be appropriately assessed. This apparatus also measures less than 5 % error between trials on the same membrane, which can be improved with more data collection for each transport measurement. Graphene is transferred onto high pore density polyimide (~50 nm pore diameter, 6E9 pores cm^{-2}) and is imaged with a scanning electron microscope (SEM) to assess graphene transfer fidelity. It is found that graphene coverage (defined as the fraction of the polyimide covered by visibly intact graphene) for samples can be as high as 98% using the transfer method explained in this work. The resulting membranes are irradiated with varying levels of Gallium ion radiation in a focused ion beam machine. It is found that irradiating the sample with ion beam settings of 8 keV acceleration voltage and a dosage of 2.53E+13 Gallium ions cm^{-2} causes no noticeable change in membrane performance of water vapor transport. Future work will include irradiating the sample at higher dosages and assessing membrane performance while correlating these dosages to what is expected in a fusion reactor setting.

Thesis Supervisor: Rohit Karnik
Title: Professor of Mechanical Engineering

Table of Contents

1. INTRODUCTION

Fusion energy is a promising form of nuclear power production that is sought after for its essentially limitless fuel supply, relatively safe operation, low land use, and minimal waste and environmental impact.[1] The main reaction of interest for fusion energy is the fusing of two isotopes of hydrogen, deuterium (D = ^{2}H) and tritium (T = ^{3}H), to form helium and a neutron (n).[1] The overall reaction is given as follows:

$$D + T \rightarrow He\ (14.1\ MeV) + n\ (3.5\ MeV)$$

The primary strategy of sustainable fusion energy is through magnetic confinement fusion in a device known as a tokamak.[2] Tokamaks are donut shaped reactors that use coils to generate strong toroidal magnetic fields which contain high temperature (over 100 million degrees Celsius) plasma consisting of superheated reactants.[2] The high pressure and temperature of the reactor make the fusion reaction above possible. Nuclear fission and nuclear fusion plants would produce the same order of power, however fusion has an inherent aspect of safety that fission does not share: if any system related to the high magnetic fields or temperatures fails, the reaction will cease.[2]

ARC (affordable, robust, compact) is an advanced fusion reactor tokamak in development at MIT (see Figure 1). For ARC, a roughly equimolar gas mixture of D and T is used as fuel. Helium produced in the reactor must be maintained below a certain threshold concentration of a few percent in order to minimize tritium inventory. Continuous operation of the reactor requires a few kg of tritium in circulation. Given the projected global inventory of tritium in 2018 is around 55 kg, tritium is considered a rare resource.[3,4] In order to minimize the amount of tritium inventory, unused DT must be separated from He and returned to the reactor. This is helpful in minimizing costs, regulatory constraints, and safety hazards of radioactive exposure as well.[5]

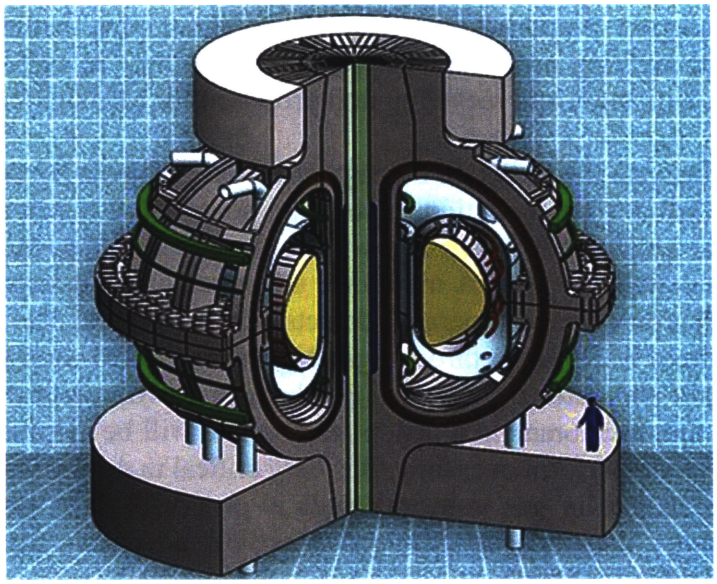

https://dotearth.blogs.nytimes.com/2015/08/11/heck-of-a-class-project-an-affordable-robust-compact-fusion-reactor-design-buildable-in-a-decade/

Figure 1: MIT-ARC Reactor Design

Membrane separation of He from $D_2/T_2/DT$ is one potential solution to removing He. Membrane based separation has benefits over other existing separation technologies including its ease of operation, cost effectiveness and low energy consumption.[6] The process stream conditions of the ARC reactor will require the membrane to maintain its integrity and performance despite irradiation from tritium decay.

Atomically thin 2D materials such as graphene have clear advantages for membrane applications and have been considered the ultimate membrane material ever discovered. It is atomically thin, allowing for the lowest possible viscous loss for fluids to pass through. It is the strongest material ever discovered (up to 130 GPa for ultimate tensile strength) allowing it to separate highly concentrated solutions with high recoverability.[7] Graphene has high chemical resistance, enabling better cleaning of the membrane and use in aggressive solvents and solutions.[8] It has extremely rigid pores ensuring uniform selectivity, and it can be customized to pass certain fluids and gases through irradiation of specifically sized pores into the 2D lattice.[9]

Research has been done on gas sieving of H_2/CH_4 using monolayer graphene, water transport through monolayer graphene using molecular dynamics simulations and experimentally using carbon nanotubes, and other gas transport through graphene oxide membranes.[10-13] However to the author's knowledge, research into membrane performance of gas transport in this radiation intensive application has not been conducted previously.

In this work, graphene is used as a model atomically thin membrane material to study the effects of radiation on membrane integrity and transport performance. Radiation from high-energy electron/ion emitting sources can break the covalent bonds in graphene, and therefore have proven effective in generating nanoscale defects and pores on the lattice.[9] Depending on irradiation conditions, these defects range from holes of a few nanometers to single-atom vacancies.[14] Analyzing defect generation on graphene and correlating the radiation damage that generated these defects with mass transport properties is essential for developing better nanopore creation protocols, and for characterizing membrane performance over time in radioactive environments such as in the tritium purification and recycling unit proposed for MIT-ARC.

This work aims to investigate the radiation damage effect on graphene by exposing this material to varying levels of Gallium ion radiation. Given the scope of this project, neutron damage experiments will not be carried out. Instead, it will be simulated by ion radiation as commonly practiced in nuclear materials research. A model for understanding the response of gas transport across graphene to radiation damage generated defects will be formed. The experiments involve gas transport in the form of water vapor through graphene subjected to varying levels of radiation. This experiment directly simulates the types of mechanisms involved in the filtration of gases through an atomically thin membrane in a fusion reactor, and will be helpful for elucidating how well these membranes could perform over time. It is very critical to determine the radiation dosage at which a noticeable change in gas transport rates is observed. This can help inform when atomically thin membranes like graphene may need to be replaced, or how they must be augmented to slow down the degradation process.

In order to measure the irradiation damage effects on gas transport through graphene membranes, we first had to design a testing method that could accurately and precisely measure gas transport through a thin membrane. Through several iterations of design, a final compact top-hat shaped

apparatus was chosen. Graphene was transferred onto high pore density polyimide (~50 nm pore diameter, 6E9 pores cm^{-2}) to allow for gas transport measurements without substantially damaging graphene. Graphene samples were imaged in a scanning electron microscope/focused ion beam machine to assess the amount of graphene coverage on polyimide after the transfer process. A transport measurement was then conducted on the sample, and the resulting transport rate was correlated to the amount of graphene coverage ascertained from imaging. The samples were then irradiated with varying dosages from gallium ions from the focused ion beam of the same machine, and the transport rates determined after each irradiation. This informs radiation damage effects on gas transport in graphene which is pivotal to designing a palladium/2D nanoporous material membrane for tritium inventory reduction in MIT-ARC.

2. MATERIALS AND METHODS

2.1 GRAPHENE TRANSFER ONTO POLYIMIDE AND POLYCARBONATE MEMBRANES

Three main base membranes (high pore density polyimide, low pore density polyimide and polycarbonate) were tested to decide which was better suited for the water vapor transport experiment (see Table 1). The processes to transfer graphene onto each were distinct. For the polyimide, we began by cutting a 10 mm by 10 mm square section of graphene on copper using a sharp razor blade. The copper square was then spin coated with poly methyl methacrylate (PMMA) coating. The spin coated copper graphene section was then etched using ammonium persulfate solution for 5 minutes. The uncoated side was placed face down in the solution. After 5 minutes, the graphene section was carefully scooped from the solution using a watch glass and placed uncoated side face down in a container of deionized (DI) water to wash off the etchant.

Membrane	Thickness (μm)	Pore Diameter (μm)	Pore Density (pores cm^{-2})	Supplier
Polycarbonate	8	0.2	-	Sterlitech
High Pore Density Polyimide	8	0.05	6E9	it4ip
Low Pore Density Polyimide	8	0.05	6E8	it4ip

Table 1: Membrane types and properties used in experiments

The sample was then transferred to another a watered down (1/3 of the original concentration) solution of ammonium persulfate, again with the uncoated side face down, and left over night. This process etched away the copper completely. The sample was then extracted using a watched glass and placed uncoated side down into a clean container with DI water to wash off the etchant. This washing step was repeated two more times. A circular polyimide wafer was then taped onto a glass slide, and the glass slide was used to scoop up the graphene sample such that the uncoated side was faced down on the polyimide. The graphene membrane was then carefully air dried on the glass slide using a cylinder of compressed air at low air velocity. The graphene was then air dried for 30 minutes in a covered petri dish, taking care to keep the sample covered so not to introduce contaminants. The sample, still in the covered petri dish, was then dried in the oven at 50 degrees Celsius for 30 minutes. After cooling to room temperature, the graphene membrane on the glass slide was submerged in acetone (acetone rinse) for 15 minutes, then 30 minutes in another fresh volume of acetone, and finally another 15 minutes in another fresh volume of acetone. The

sample was then submerged in ethanol as a final rinse, and then dried in a covered petri dish (See Figure 2). Lastly, the sample was dried in the oven at 130 degrees Celsisus for 30 minutes.

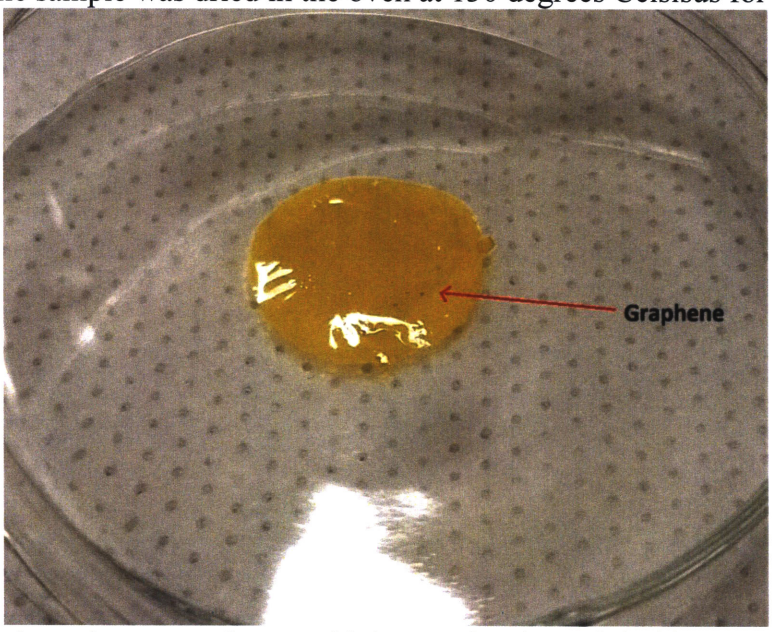

Figure 2: Completed graphene transfer onto high pore density polyimide membrane

The polycarbonate transfer method was similar in the first step of cutting the section of copper etched with graphene but differed subsequently. The graphene on one side of the sample was back-etched away in ammonium persulfate solution for 7.5 minutes. The sample was then extracted using a watch glass and washed in DI water by placing the etched side face down in the water for 10 minutes. This was repeated in fresh DI water two more times. While this was occurring, we soaked a fresh polycarbonate membrane in isopropanol for 15 seconds and let dry in order to clear membrane of contaminants. We formed a stack from top to bottom of a glass slide, weighing paper, polycarbonate (shiny side up), graphene sample (etched side down), weighing paper, and another glass slide. We used a glass pipette to apply pressure to the top glass slide by rolling the pipette over the slide. We used care to firmly but not excessively apply pressure to the whole slide but focused on the component directly above the polycarbonate and graphene. We flipped the whole sandwich of components. Using the bottom slide, we placed the paper with graphene and polycarbonate (graphene side down) into the ammonium persulfate etchant. We pulled away the paper after sinking, and the graphene sample was bonded to the polycarbonate membrane without the presence of air bubbles between them. We let the sample etch overnight, and then rinsed using DI water wash explained earlier. The graphene membrane was then prepared for transport measurements (see Figure 3).

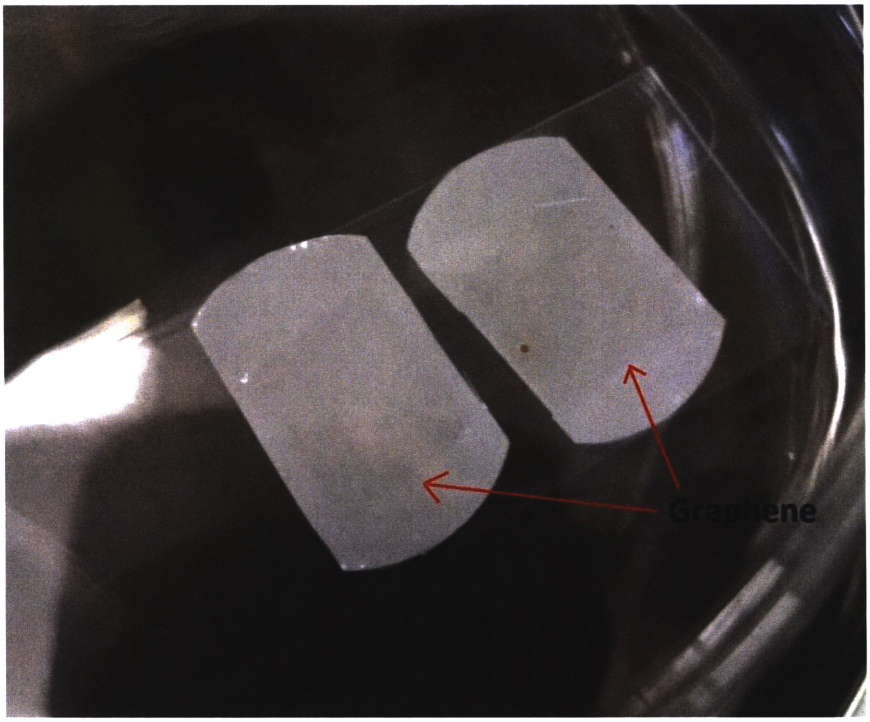

Figure 3: Completed graphene transfer onto polycarbonate membrane

2.2 ASSESSING TRANSPORT RATES

Water vapor transport through the membrane film was quantified in terms of the mass of water evaporating from a closed vessel that allowed water vapor to escape only through a membrane (see Section 2.4 for different apparatus designs). The technique for measuring mass flow rate of the water vapor was by repeated weighing of the vessel containing liquid DI water which evaporated over time. Water vapor was formed through water molecules acquiring enough energy to break the intermolecular bonds and escape the surrounding liquid; the partial pressure of water vapor next to the water interface was determined by the water temperature. The membrane was placed above the vessel such that the water vapor could only primarily leave the system by passing through the membrane. The membrane was tightly pressed to the water vessel allowing for minimal leakage. The weight in grams and time of weighing was recorded at each measurement. Measurements were usually taken over the span of a couple hours to days depending on the apparatus used. The final apparatus used only required the span of a few hours to run a test.

The mass flow rate was extracted from the data using the degree one polynomial regression fit in MATLAB's curve fitting toolbox. The magnitude of the slope of the line of best fit was the mass flow rate (see Figure 4). Half of the width of the 95% confidence intervals provided in the slope estimate was used as the error on the slope, and thus the error on the mass flow rate for a single transport experiment. The data followed a linear pattern over durations where a large amount of liquid was still present in the vessel as to not distort the inner flow resistance of the vessel. Thus, it was assumed that the transport rate would be a constant value over these durations.

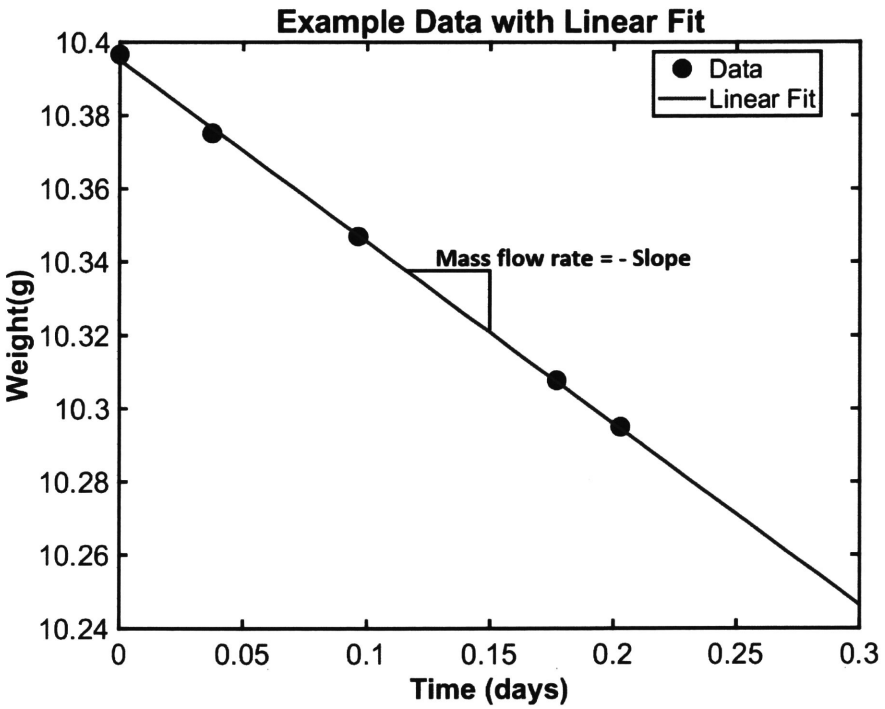

Figure 4: Example of transport measurement data and a line fit to the data to show how mass flow rate is extracted

The mass flow rate was measured in g/day given we are only measuring a small liquid volume change due to restrictions of membrane size. The membrane area was not used to normalize the flow rate given the same membrane area was used for each measurement. Also, this work concerns relative changes in flow rates due to irradiation conditions, which helps assess membrane performance.

A primary obstacle of this research was performing accurate and repeatable measurements of the mass flow rate. Large variances in the data caused the slope measurement or mass flow rate to have large error. Given we are tried to perceive potentially minute changes due to irradiation, large variability was unacceptable due to the large errors that would result. Many iterations of apparatus designs were carried out to minimize this variability. One unavoidable limit was the balance used which had a precision of 0.0001g. However, if necessary a more accurate balance could be used. Ultimately, it was decided that minimizing the weight of the vessel, reducing the amount of readjustments to the vessel during weighings and reducing the flow resistances of inside the vessel and outside the apparatus above the membrane were the most important factors in consistent measurements.

2.3 RESISTANCE MODEL OF FLOW

The system of water evaporating inside of a chamber and passing through a membrane to the environment was approximated with the following flow resistance model:

$$Q = \frac{\Delta p}{R_{total}}$$

Where Q equals the flow rate in m^3/s, Δp was the water vapor partial pressure differential in Pa between the inside and outside of the membrane, and $R_{total} = R_{in} + R_{film} + R_{out}$ was the total resistance to flow of water vapor from the water pool to the outside of the membrane in kg/m^4*s.[15] This was a very simple model, so this model was appropriate for the temperatures (25 degrees Celisus) and flows (1 g/day) we were concerned with (see Figure 5). In addition, this model was used to gain an understanding of membrane performance, and resistance itself was not being measured. The goal in designing the testing apparatus was to reduce the magnitudes of R_{in} and R_{out} in order to better observe changes in membrane resistance.

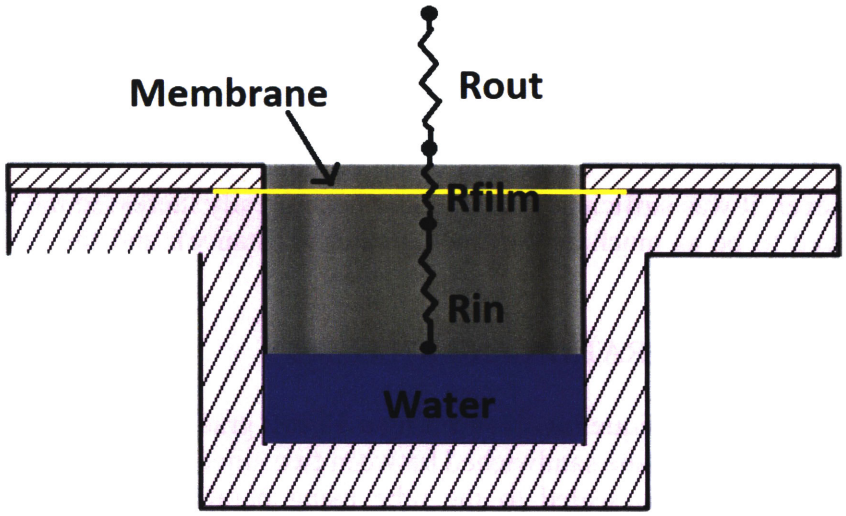

Figure 5: Resistance model for gas transport from water pool through the membrane to the outside environment

To reduce R_{in} as much as possible, a magnetic stir bar was placed inside the device in the water pool such that the water-air interface was broken up and that the air directly above the water was not stagnant. The stir bar also functioned to maintain the water pool at a uniform temperature. Additionally, the thickness of the disk was minimized to 1 mm to prevent stagnant air above the membrane and the whole apparatus was placed in the fume hood where air flow was present. This helped to minimize R_{out}.

Δp was dependent on the liquid temperature as this temperature determined the vapor pressure at the surface of the liquid.[16] Under the same test conditions, it was assumed liquid temperature will be the same, and thus Δp would be constant between test runs of the apparatus with different membranes. Also it was assumed inner and outer resistances were constant with constant test conditions. Thus to explain the differences in flow rates, different membrane resistances were assumed. Our baseline membrane used in this study was an 8 micrometer thick bare polyimide membrane that had 50 nanometer pores at a pore density of 6E9 cm^{-2}.

A transport measurement using the device above resulted in a water vapor transport rate of roughly 1 g/day. Using a similar membrane with 10 times less pore density we measured roughly 0.6 g/day for water vapor transport. It was assumed that the 6E8 cm^{-2} low pore density polyimide membrane had 10 times more resistance to flow than the high pore density polyimide. Since $\Delta p = QR_{total}$ and Δp was assumed constant between different membranes, we could assess how large the inner and

outer resistance were compared to the membrane resistance. The following equations showed the steps towards determining the relationship between $R_{in} + R_{out}$ and the resistance of the high pore density polyimide:

$\Delta p_h = \Delta p_l$, where h denotes high density polyimide and l denotes low density polyimide

$$Q_h(R_{in} + R_{out} + R_{film})_h = Q_l(R_{in} + R_{out} + R_{film})_l$$

$$R_{in} + R_{out} = \frac{\left(A - \frac{Q_h}{Q_l}\right)}{\frac{Q_h}{Q_l} - 1} R_{film_h}, \text{ where } (R_{film})_l = A(R_{film})_h \text{ and A is a scalar}$$

For the results presented above, we get that $R_{in} + R_{out}$ is 12.5 times the resistance of the high pore density polyimide film. This was the best that could be done given the experimental setup and limited time. However, it was sufficient since the graphene greatly increased the resistance of the membrane (observed to be as much as 24 times greater resistance), and the change was easily observed.

2.4 APPARATUS DESIGN ITERATION AND SELECTION

Initially, the measurement technique involved filling a 15 mL graduated test tube with 11 mL of DI water and placing the membrane sandwiched between two silicone gaskets on top of tube. The membrane/gasket sandwich was sealed to the tube using parafilm, and the tube was partly submerged in a 50 degree Celsius water bath to speed up the evaporation rate of the liquid DI water. Three test tubes with different membranes were tested at a time in order to have a control measurement between successive tests. The whole apparatus was placed inside a fume hood so as to minimize particulate that could contaminate the membranes and also to lower the outer resistances of the gas transport (see Figure 6). The weight of the tube and contents was recorded once per day, and the mass flow rate extracted from the slope of the data.

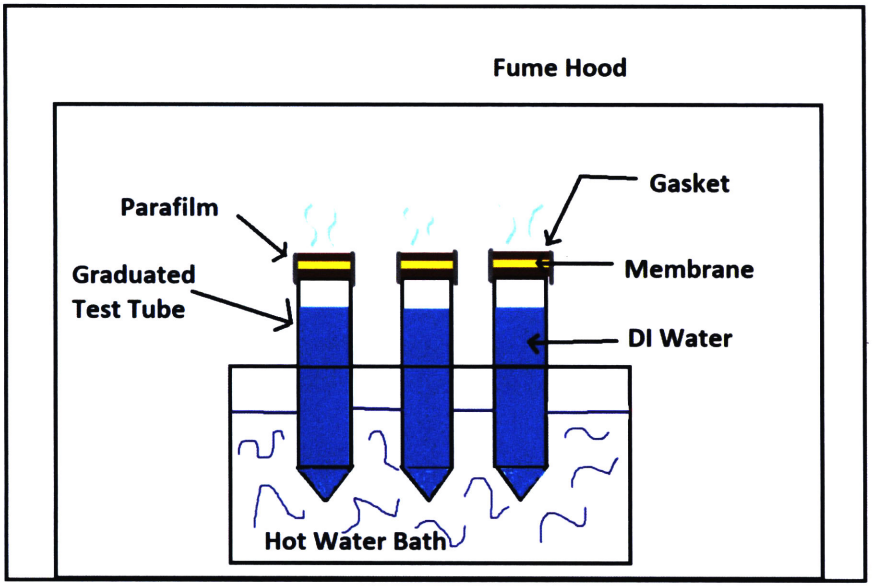

Figure 6: Graduated test tube set up in fume hood with hot water bath set to 60 degrees Celsius
The results for trials with graphene, bare PI and a 30 keV electron beam irradiated graphene are tabulated (see Table 2). The results show that bare polyimide (PI) has a lower transport rate than the irradiated graphene membrane which should not be the case. The bare or uncovered PI should offer the least resistance to flow and thus should have the highest transport rate.

Membrane	H_2O transport rate (g/day)	
	Trial 1	Trial 2
Bare High Pore Density Polyimide	0.176 ± 0.037	0.146 ± 0.010
High Pore Density Polyimide + Graphene	0.128 ± 0.023	0.107 ± 0.031
30 keV irradiated polyimide + graphene	0.212 ± 0.025	-

Table 2: Transport Results from Graduated Tube Apparatus with membrane area ~50 mm^2

The issue with this method was the large mass of the tube and water compared to the amount of water actually leaving the tube (17 grams versus 0.14 g/day). This made it challenging to acquire consistent measurements given the precision of the scale. The placement of the tube in the hot water was not rigid and repeatable resulting in varied orientations, which in turn could lead to differing transport rates between measurements. Also, applying the parafilm to seal the tube and membrane distorted the membrane potentially damaging the graphene on top or, if it was not sealed well enough, allowed for leakage. This could result in misleading results. These issues could explain why the results were unexpected, and motivated the development of a new method to measure transport.

The second apparatus attempted was using PermeGear franz cells with orifice diameter of 9 mm and spherical diameter of 18 mm. These cells allowed warm water acting as a heat source to flow around the vessel containing the 0.75 mL of DI water. This method involved clamping the membrane between the cell top and body with no need of parafilm to seal. Tubes passed water from a hot water bath set at 50 degrees Celsius into the franz cells and back into the bath using a peristatic pump (see Figure 7). Before weighing the franz cell, the pump was shut off and tubes disconnected, and ethanol and compressed air was sprayed into the jacket section in order to speed up evaporation of left over water in the jacket. Three cells were used at once to allow for controls, and the apparatus was placed in the fume hood as before. The device was an improvement over the previous method given the clamp did not distort the membrane. The device also resulted in the water evaporating in the same orientation each time, so the transport rates would be more consistent between measurements.

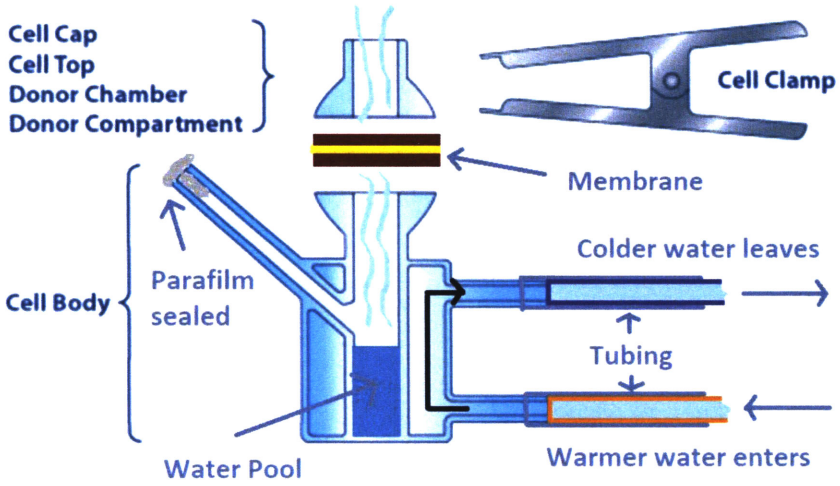

https://permegear.com/parts-of-a-franz-cell/

Figure 7: Franz cell setup with flowing water from peristatic pump

Tests were carried out on polycarbonate and high pore density polyimide membranes and the results show large variations in the transport rates (see Table 3). Temperature differences between the heated water going into each cell were no more than 2.1 degrees Celsius, so it was assumed this would not lead to large variation between transport rates on different cells.

Sample	H_2O Transport Rate (g/day)		
	Trial 1	Trial 2	Trial 3
Polycarbonate 1	0.18 ± 0.16	0.209 ± 0.085	-
Polycarbonate 2	0.195 ± 0.058	0.220 ± 0.076	0.249 ± 0.071
Polycarbonate 3	-	-	0.236 ± 0.086
Polycarbonate 4	-	-	0.250 ± 0.079
Polyimide	0.231 ± 0.017	0.177 ± 0.034	-

Table 3: Franz cell apparatus with flowing heated water tests on different membranes of membrane area ~50 mm^2

The franz cells were heavy (~ 90 grams) and water remaining in the flowing jacket component varied in amount, even with measures taken to remove it, which resulted in overlapping error bars between the samples. The amount of water evaporated between measurements was not vastly higher than the amount of water fluctuation in the heated component. Thus, it was difficult to distinguish between the measurements and achieve repeatable results.

A variation on this method was using a separate vessel made from a straw and parafilm and placing this vessel inside of the fluid measurement device. The vessel was filled with 0.9 mL of DI water, and at each measurement the membrane was taken off, and the vessel removed to weigh. This method involved weighing a very light vessel, removing the issue of large weight distorting the changes. Tests using this new method were carried out on uncovered polycarbonate membranes

and graphene-covered polycarbonate membranes giving similar transport rates for covered and uncovered samples, which is unexpected (see Table 4).

Sample	H_2O Transport Rate (g/day)
Polycarbonate Plain 1	0.248 ± 0.032
Polycarbonate Plain 2	0.241 ± 0.034
Polycarbonate Plain 3	0.236 ± 0.036
Polycarbonate-Graphene 1	0.220 ± 0.025
Polycarbonate-Graphene 2	0.204 ± 0.016
Polycarbonate-Graphene 3	0.268 ± 0.051

Table 4: Transport results of graphene covered and uncovered polycarbonate membranes using Franz Cell Apparatus with separate straw weighing vessel and membrane area ~50 mm^2

There was a significant improvement in variation on the transport rate (highest variation is now 20 % versus 90 %). The results showed that the transport rates were roughly the same across the samples. The transport rates with and without graphene were similar for unknown causes, so it was decided to reduce the variability in testing conditions between cells.

To remove the heating variability between cells, the same set up was attempted but with no circulating water, and instead placing the cells inside an oven at uniform temperature of 50 degrees Celsius to stimulate evaporation. Instead of a straw as a vessel, a pipette tip stuffed with parafilm to prevent water leakage was used. The vessel was filled with 0.5 mL of DI water in each test. A control of no membrane was tested in addition to graphene covered and uncovered membranes. Again, the results from no membrane, membrane, and membrane plus graphene were indistinguishable (see Table 5).

Sample	H_2O Transport Rate (g/day)		
	Trial 1	Trial 2	Trial 3
Polycarbonate 1	0.533 ± 0.072	0.556 ± 0.067	-
Polycarbonate 2	0.593 ± 0.090	0.604 ± 0.076	-
No Membrane	0.558 ± 0.098	0.625 ± 0.089	-
Polycarbonate + Graphene 1	-	-	0.605 ± 0.067
Polycarbonate + Graphene 2	-	-	0.560 ± 0.052
Polycarbonate 3	-	-	0.577 ± 0.096

Table 5: Franz cell oven test with graphene membranes, plain membranes, and no membranes with membrane area of ~50 mm^2

This indistinguishability between no membrane, membrane, and membrane with graphene were likely resultant of the inner flow resistance of the measuring vessel being extremely large such that it bottle-necked the water vapor transport rate. This was due to the air beneath the membrane being relatively stagnant and diminishing flow. To correct this, a new apparatus was designed and 3D printed with high temperature resin that allowed for stir bar placement inside of the apparatus to provide some turbulence to the air around the water vessel but beneath the membrane. Another stir bar was placed inside the water vial to stir the air above the water-air interface and keep the water at more uniform temperature also helping to lower transport resistance (see Figure 8).

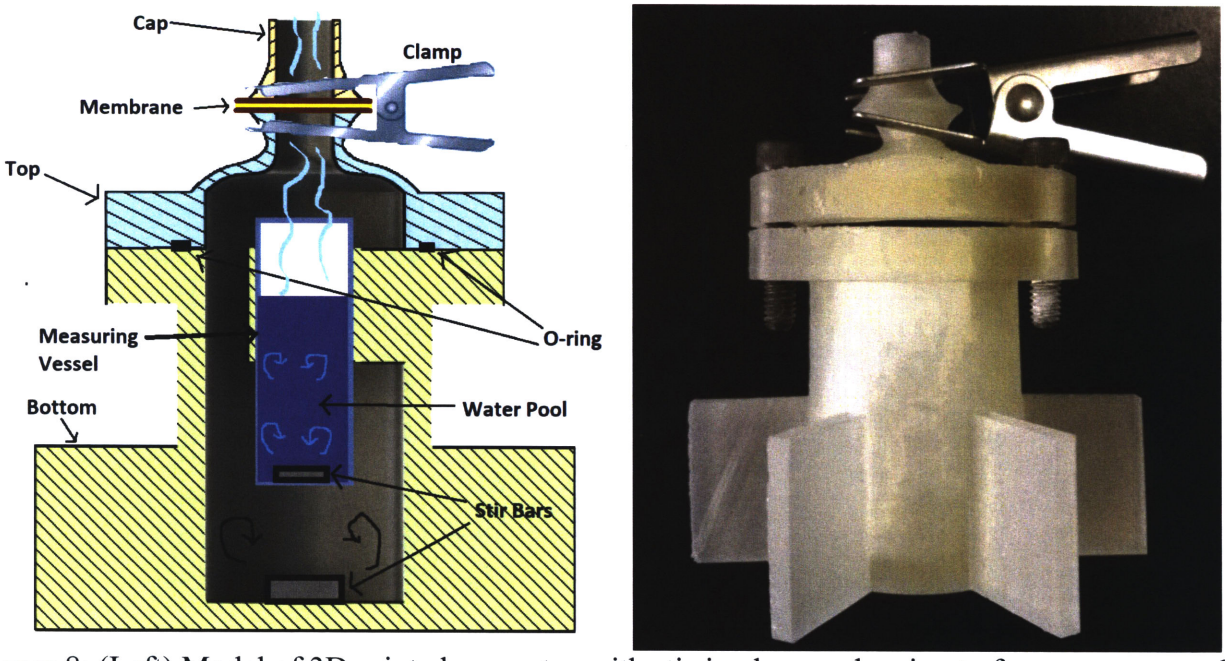

Figure 8: (Left) Model of 3D printed apparatus with stirring bars and o-ring to form pressure seal between top and bottom components. (Right) Actual printed and tested apparatus

Using this device by placing it on a heated stir plate, and separately measuring the vessel of DI water, large error in the measurement was observed. The potential cause of this was due to removing the membrane at each measurement. Any vapor pressure developed between measurements would be immediately diminished upon removal of the membrane, and so each measurement involved some lag time. Additionally, the inside chamber of the device beneath the membrane was curved, allowing for evaporated water to collect and condense against the walls of the container without passing through the membrane.

To mediate this a device was designed to be small and compact so that the water can be contained inside, and each time the whole device weighed. This device, similar to a top hat in shape, was made out of non-magnetic aluminum material and was filled with a stir bar and water, and covered with the membrane (see Figure 9). The membrane was sealed to the device, by screwing a disk on top of the membrane into the bottom vessel to finger tight pressure. Additionally the area of the membrane exposed to the air was greatly increased from ~50 mm^2 to ~125 mm^2. The chamber vessel was designed to be cylindrical and the same diameter as the membrane opening so that there was more of a direct path for the water vapor to go passing through the membrane. The apparatus was placed on a stir plate inside of the fume hood.

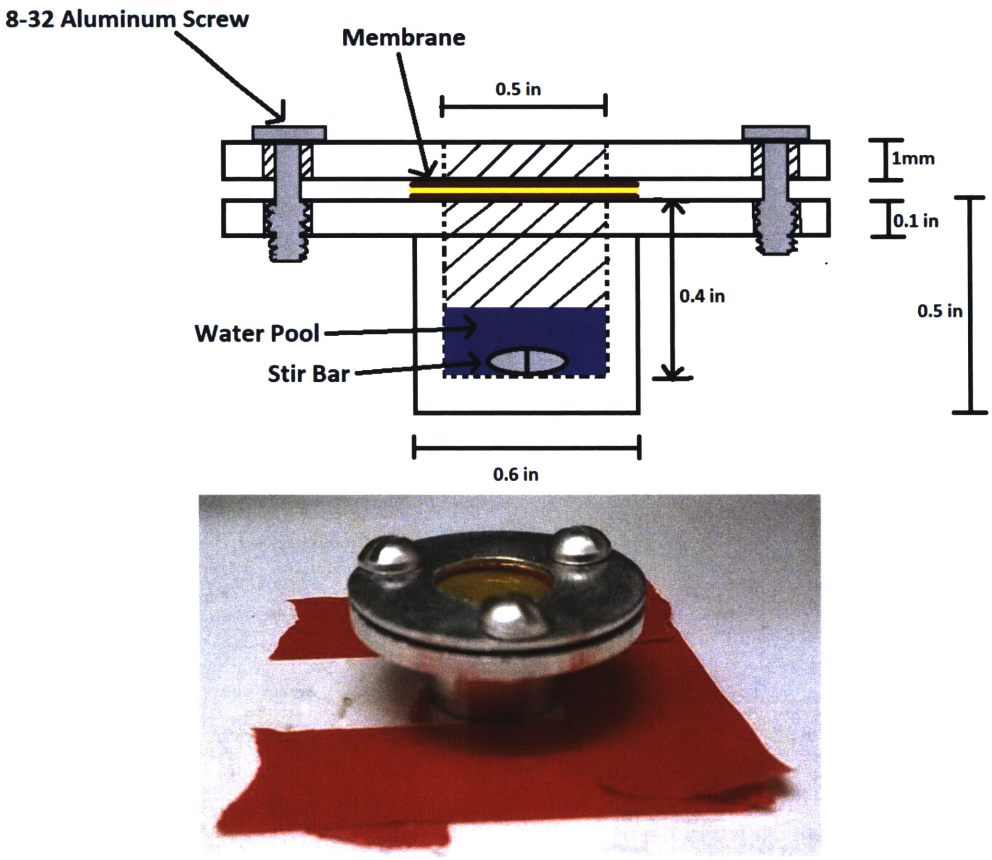

Figure 9: "Top hat" apparatus design where whole device is weighed and a stir bar is present

This apparatus was airtight when sealed (only 0.0092 ± 0.0039 g/day water vapor transport with "impermeable" parafilm membrane). The stir bar coupled with the increased diameter vessel size reduced the inside flow resistance of the apparatus, and using the fume hood and a thin cover, the outside flow resistance was reduced as well. Initially, the apparatus was heated to 60 degrees Celsius using the stir plate. With no membrane, stir rate of 240 rpm, and initial water pool size of 0.3 mL, the mass transport rate was 2.388 ± 0.093 g/day. It was decided to increase the stir rate to 600 rpm and initial water pool size to 0.5 mL, resulting in a mass transport rate of 6.416 ± 0.334 g/day. This allowed for higher initial transport, and thus more of noticeable change in transport when adding graphene.

Similarly, we saw a higher mass transport rate of 1.470 ± 0.111 g/day with high pore density polyimide than 1.265 ± 0.020 g/day with polycarbonate. Thus, the high pore density polyimide was chosen as the testing membrane that was used for the irradiation investigation. Since adding graphene to the high density polyimide resulted in the largest change in transport rate, and would allow for more discernable differences in transport rate when subjected to different radiation conditions.

The heating of the apparatus at 60 degrees Celsius using the stir plate led to a large temperature differential of 10 degrees Celsius between the water pool and the apparatus. We were concerned that this temperature gradient could be dominating the flow rate through the apparatus, regardless

of membrane resistance, so we decided to no longer heat the device. The non-heated stir bar device consistently results in low error (less than 10 percent) and displays behavior as expected according to resistance models (see Table 6).

Sample	H_2O Transport Rate (g/day)	
	Trial 1	Trial 2
High Pore Density Polyimide 1	1.043 ± 0.020	1.08 ± 0.13
High Pore Density Polyimide 2	0.939 ± 0.068	-
Low Pore Density Polyimide 1	0.630 ± 0.020	-
High Pore Density Polyimide + Graphene 1	0.3845 ± 0.0060	-
High Pore Density Polyimide + Graphene 2	0.495 ± 0.023	-

Table 6: Aluminum Apparatus tests of high density PI, low density PI, and graphene covered high pore density PI with no heat source and with membrane area ~125 mm^2

The low pore density PI, which had 10 times fewer pores than the high pore density PI, would likely have 10 times higher resistance than the high density PI. This was reflected in the significant drop in transport rate from 1.0430 g/day to 0.6304 g/day when using low pore density PI instead of high pore density PI. Additionally, graphene should increase membrane resistance by an order of magnitude or more as well, so the data reflected this with a large decrease in transport rate with the addition of graphene. Additionally, after running a transport measurement test four times on the same high pore density polyimide sample, the average mass transport rate was given by 0.7433 ± 0.0361 g/day, which is an acceptable 4.85 % error. Previous results for that specific membrane was around 1 g/day so it is believed that the membrane was contaminated. These clearly distinguishable changes that align with our expectations about the transport model show that this apparatus works and provides repeatable results. It will be sufficient for investigating the irradiation damage effects on graphene.

3. IMAGE ANALYSIS TECHNIQUE

3.1 ASSESSING SAMPLE PORE DENSITY

Prepared high pore density polyimide membrane graphene samples were imaged in an FEI Helios NanoLab 600 DualBeam Focused Ion Beam (FIB) machine. The membrane was secured to an imaging stage using copper pins which also helped conduct built up charge away from the sample. The copper pins also helped to reduce drift in the image, allowing high resolution photographs of the nanopores to be taken. The sample and stage were then loaded into the machine and imaged using the scanning electron microscope (SEM) component of the NanoLab. ipPORE, the manufacturer for the polyimide membranes, lists the high pore density polyimide at a pore density of 6E9 cm^{-2}, but the actual pore density differs. The pores were enhanced and counted using image processing techniques. The techniques and specific functions in MATLAB called would vary depending on the image. In general, the contrast in the image was enhanced, and the function imfindcircles() was used to locate all of the pores and demarcate them with a blue marker (see Figure 10).

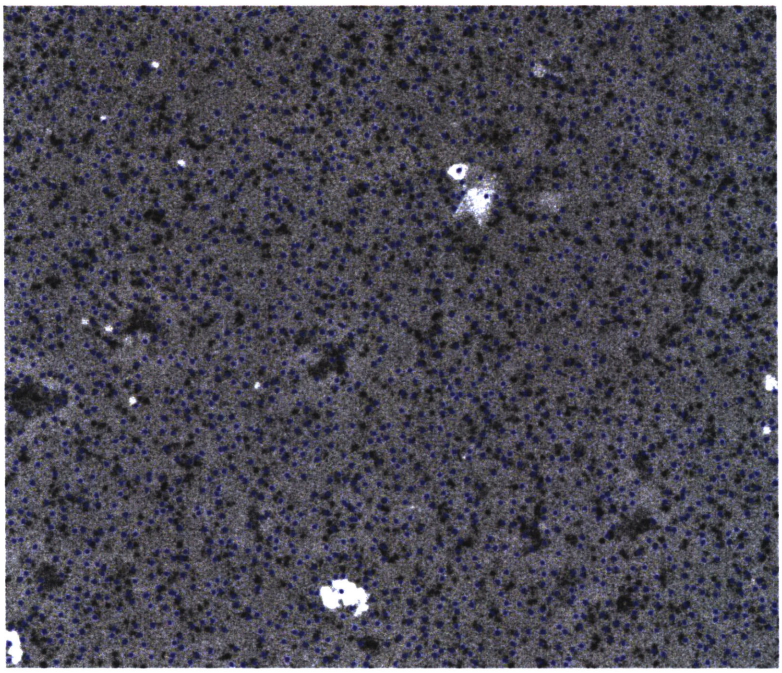

Figure 10: Graphene image with pores marked with a blue marker for pore density calculation

The number of pores/circles found would be verified by eye to ensure the blue dots and pores mostly match up and few pores are missed. The number of pores calculated by MATLAB was then divided by the area of the image to get the pore density. The area of the image is found from first estimating the size of a pixel and then calculating the length and width of the image. For the image above, the pore density estimated was 3.26E9 cm^{-2}, and the average for the sample was 3.40 ± 0.25E9 cm^{-2}. This is roughly half the density of what was nominally listed but still on the same order of magnitude. Thus, the pore density for each polyimide membrane has some variability. Thankfully, the resistance of graphene was so large that it could mask this discrepancy.

3.2 ASSESSING GRAPHENE COVERAGE

Imaging the graphene samples to get an assessment of graphene coverage of the sample was essential to validate that the method of graphene transfer was indeed working and to correlate the transport rate observed to graphene coverage on the sample. The same SEM machine was used to image the samples for graphene coverage as above. The graphene was electrically conductive and so would not accumulate vast amounts of charge since the electrons had a path to travel to ground.[8] Thus, the charged areas of the sample appeared lighter and more visible and the areas where graphene covers the sample were darker in the SEM. The edge of the sample could be located in the SEM, and various parts of the graphene sample could be observed to check for defects. Defects would appear grey to bright white in color. Pores uncovered by graphene appeared as a black hole surrounded by a bright white ring (see Figure 11).

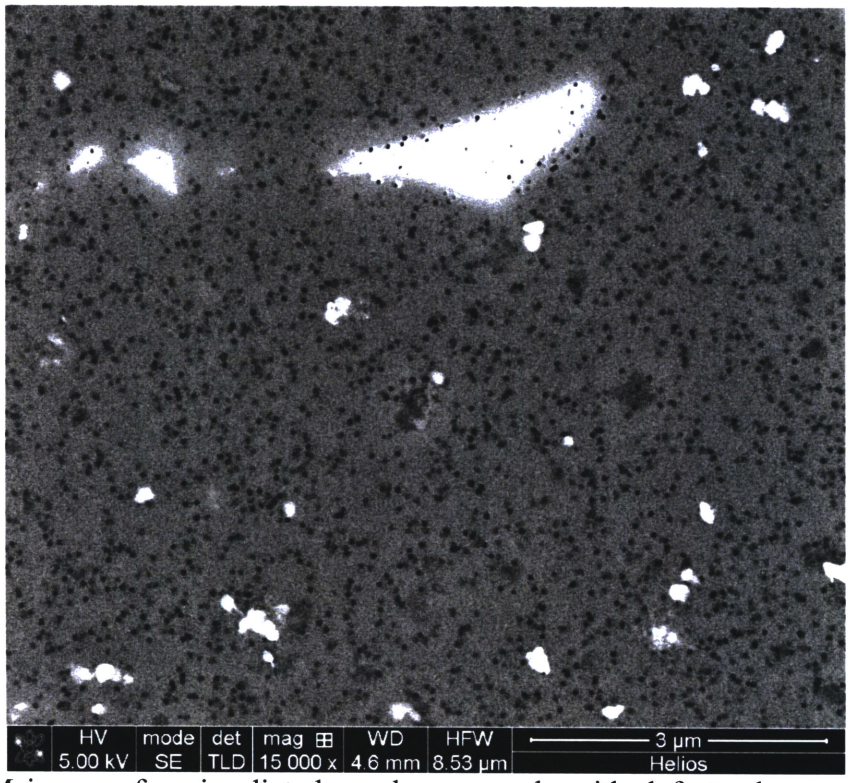

Figure 11: SEM image of un-irradiated graphene sample with defects shown clearly in bright white, and uncovered pores within these areas are dark holes with bright white surrounding the edge

Several locations on each graphene sample were imaged. The white uncovered areas and area covered in contaminant on the graphene were enhanced using MATLAB's image processing toolbox. It was assumed that the areas covered by dust particles or other contaminants were damaged and thus there was no graphene coverage there. To determine the area uncovered by graphene in the image, we first converted the image to greyscale using MATLAB's rgb2gray() function. Next, we set a pixel value threshold between 0 and 255, that for every pixel with a value greater than said threshold, the pixel was converted to a Boolean 1 corresponding to white or true. For every value lower than the threshold, the pixel was converted to boolean 0 corresponding to black or false. The threshold value was adjusted so that the black white image resulting from the Boolean conversion overlapped well with the unaltered image with respect to defects and contaminants (see Figure 12).

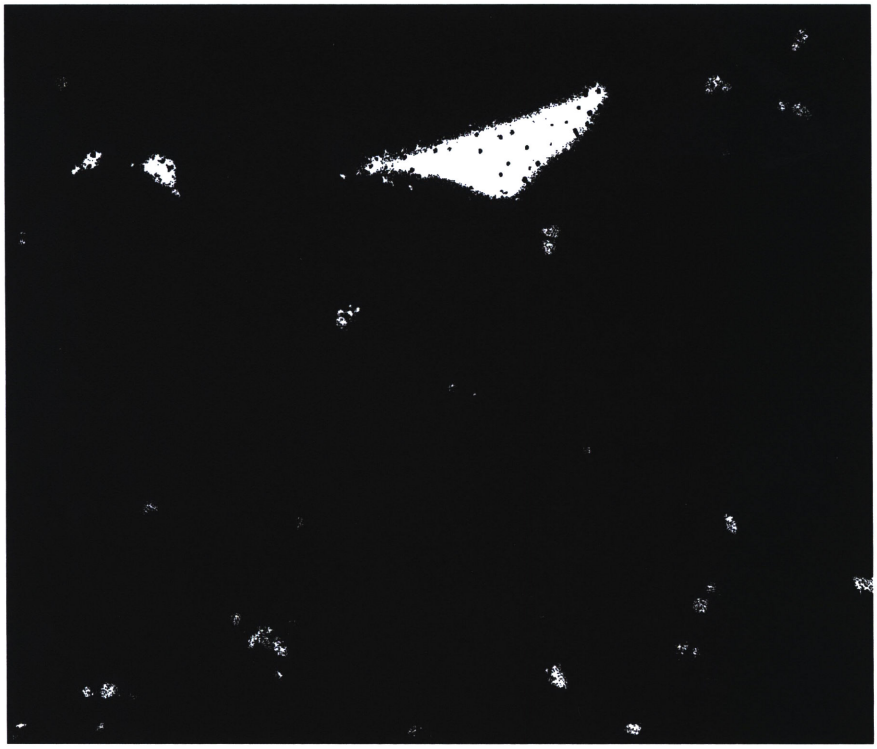

Figure 12: Black White Boolean image corresponding to 95 pixel value threshold for Figure 11 where white colored regions are all defects or contaminants

The total number of pixels of white space out of the total number of pixels of the image gave the percentage of sample area uncovered by graphene. The image above corresponded to 3.75 ± 0.50 % uncovered area. For this particular graphene sample eight images were analyzed. The resulting average percent uncovered area for the sample was 5.82 ± 6.17%. This sample was not used in the water vapor transport measurement.

3.3 GRAPHENE COVERAGE FOR PRE-IRRADIATED SAMPLE

This method was improved by better randomizing the location of the images and increasing the overall size of the image taken from 10 μm by 10 μm to roughly 100 μm by 100 μm. On another sample used in the actual transport measurement, seven large scale images were taken. The corresponding average uncovered area of the sample was given as 2.43 ± 1.01%. A typical example of the graphene coverage for this sample was provided by the following figure which shows the unaltered and Boolean image (see Figure 13).

Figure 13: Graphene sample image with 1.12% area uncovered by graphene.

On the large scale of 100 µm by 100 µm, this was the typical image seen of a well-transferred graphene sample. On a smaller scale, defects can appear larger and more prominent and can skew perception on graphene coverage of the sample (see Figure 14).

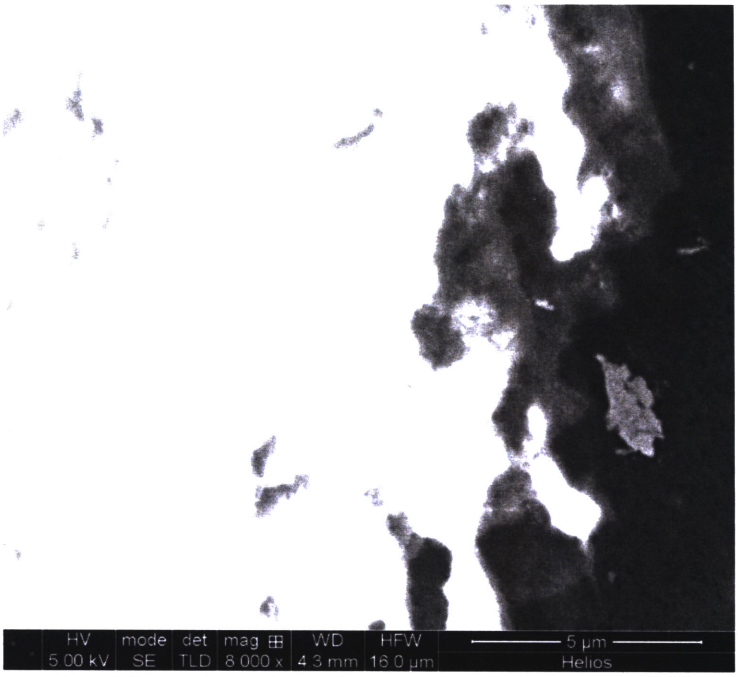

Figure 14: Close up roughly 15 µm by 15 µm image of same sample as Figure 14.

Clearly the above image demonstrates if the image was too small, graphene damage would appear more widespread than is actually the case. This image showed 67.07% area uncovered by graphene which would certainly skew the average calculated from the larger samples. Additionally, if the image was too small, there was a higher chance of finding these defect heavy locations as one randomly selects where to image. It was best to take larger images. Also important was imaging

away from the edges where defects are more likely to be present due to securing the sample down to the stage for imaging in the SEM and other consequences of handling.

Using image analysis to assess irradiation damage was not as straight forward. Nanoscale defects such as single atom vacancies could form in the graphene, but these would be beyond the resolution of the SEM/FIB machine used for this work.[17] At larger dosages of radiation, defects could accumulate and larger tears in the graphene may form which could then potentially be observed in the SEM.

4. IRRADIATION OF GRAPHENE SAMPLES

The graphene membranes were irradiated with varying dosages in order to assess how much radiation damage affected the transport properties of the membranes. The ion beam component of the FIB Helios machine irradiated the sample with gallium ions. The beam could irradiate a 1.28 mm by 1.77 mm rectangular section of the sample, so the beam was focused on multiple points in the sample in order to irradiate the whole graphene surface. The sample was irradiated, and afterwards a water vapor transport measurement was taken.

Initially, an un-imaged sample was irradiated in the FIB with the beam settings at 8 keV acceleration voltage, beam current of 1.6 nA, and beam density of 4096 by 3536 pixels and dwell time of 1 microsecond (meaning each roughly 0.432 μm by 0.432 μm pixel was irradiated for 1 microsecond). This corresponded to a dosage of 2.13E+12 Gallium ions cm^{-2} at 8 keV acceleration voltage. The pre-irradiated transport measurement for this sample gave a mass flow rate of 0.3845 ± 0.0060 g/day. We used the result from Chapter 3 for interior and exterior flow resistance versus membrane resistance to calculate the resistance ratio between graphene with membrane and membrane alone.

$$12.5 = \frac{\left(A - \frac{Q_h}{Q_l}\right)}{\frac{Q_h}{Q_l} - 1}$$

Where $R_{graphene} = AR_{film,h}$, Q_h equals the mass flow rate for high density PI alone, and Q_l equals the mass flow rate for the graphene with high pore density PI. Q_h was not specifically measured for this particular sample, however it was assumed to be around 1 g/day since other high pore density PI membranes were measured close to that result. Using the pre-irradiated mass flow rate above, we found that this sample of graphene with high pore density PI was roughly 24 times more resistant than high pore density PI alone.

Post irradiation, the transport measurement gave 0.3664 ± 0.0119 g/day. Multiple measurements were not taken pre and post irradiation, however given the measurement variability was less than 5 %, it was assumed multiple measurements would give an average significantly close to what was found with one measurement. The pre and post irradiation transport rates were not significantly different, and additionally the post-irradiation measurement was lower in magnitude than the pre-irradiation measurement. This signifies that an insignificant amount of radiation damage was done to the sample, motivating a higher dose of irradiation for the next sample.

A second un-imaged sample was irradiated with similar beam settings as above except at a much higher beam current of 19 nA corresponding to a dosage of 2.53E+13 Gallium ions cm^{-2}. The transport rate of water vapor prior to irradiation was given by 0.4954 ± 0.0227 g/day. The graphene coverage for this sample was worse than the previous sample, however this particular graphene sample still provided a resistance roughly 14.75 times greater than high pore density PI alone using the same calculations as above. This 14.75 times increase in resistance was sufficiently significant that it reflected noticeable difference between undamaged graphene and no graphene.

After irradiation, the transport rate of this second sample was measured three times giving an average mass flow rate of 0.5934 ± 0.0149 g/day. This was significantly different from the pre-irradiated results, so it was assumed that the graphene was damaged in some capacity by the FIB. It was decided to irradiate the second sample again with the same beam settings thereby doubling the radiation dosage provided to the sample. Two transport measurements were conducted on this second sample giving 0.4612 and 0.467 g/day respectively. This apparent increase in resistance was surprising. It was thought that particulate and contaminants dirtied the sample leading to more blockage of PI pores. The sample was washed in isopropanol for 10 minutes to clean the sample, and a transport measurement was conducted again. This time the transport rate increased to 0.5241 ± 0.0462 g/day. There was most likely some particulate dirtying the sample, however this transport rate was still less than the transport rate of the sample after one irradiation. It was uncertain whether the current radiation dosage was actually damaging the graphene significantly.

A third graphene sample was prepared and imaged first prior to taking a transport measurement or irradiating. The images were shown in the later part of Chapter 4. The percentage area of the sample uncovered by graphene was measured to be 2.43 ± 1.01 %. A transport measurement on this sample was taken three times prior to irradiation. The resulting mass flow rate was 0.5343 ± 0.0477 g/day. Again using the calculations for graphene resistance relative to high pore density PI alone, we see that this sample of graphene with high pore density PI has a resistance roughly 13 times greater than the high pore density PI alone. This demonstrates that the first sample with a higher resistance most likely had higher graphene coverage than this second or third sample since it had a higher membrane resistance.

The third sample of graphene and high pore density PI was then irradiated with the same beam settings as above at 19 nA. However, the sample was irradiated twice in one go, providing twice the dosage. Three transport measurements were conducted on the sample giving an average mass flow rate of 0.5597 ± 0.0232 g/day. This value was not statistically significant from the un-irradiated result which infers that both this sample and the second sample were not significantly damaged by the applied radiation dosage from the FIB. This was positive since a substantial amount of radiation was applied to the graphene without diminishing the performance of the membrane.

The third sample was reimaged after the irradiation, and shown to have 2.25 ± 0.65 % area uncovered by graphene. This was not statistically significant from the results prior to radiation, which could explain why there was no distinguishable difference in membrane performance before and after irradiation. The first graphene sample was imaged after irradiation, and was found to have 2.42 ± 0.38 % area uncovered by graphene. This graphene coverage was also not significantly different from the results for other samples, so there must have been other defects in the sample

that could not be perceived by the SEM. Potentially there were many nanotears in the sample that could not be imaged by the SEM that would describe the graphene coverage as worse than what was observed in the images.

5. CONCLUSIONS AND FUTURE WORK

This work provides a foundation for future experiments in the Karnik lab measuring gas transport across thin membranes. The top-hat apparatus designed is effective in demonstrating significant changes between membranes with and without graphene present. The mass transport rates are measured to be roughly 1 g/day without graphene and 0.5 g/day with graphene with an error less than 5 %. The results primarily used four data points to extract a mass transport rate, so the error will significantly improve as more data points are taken in each experimental run.

The current top hat apparatus provides an outside and inside resistance equal to 12.5 times the resistance of the high density polyimide film. Moving forward the apparatus could be modified to lower this ratio. A design with lower temperature variation between the apparatus and the liquid water could help to increase the effect of the membrane resistance on flow. This could involve the addition of porous fins inside the vessel that holds the water to increase heat transfer between the apparatus and the liquid. Additionally, the apparatus material could be made from a more thermally conductive material like copper. More turbulence to the air inside the device from a larger stir bar could also decrease the inner resistance. Better air flow over the top of the apparatus using a stronger fan for example could help decrease the outside resistance of the membrane.

An aspect of concern regarding the device is that the membrane tenses as the top disk is secured to the bottom of the apparatus with screws. Although the transport results were similar after repeated releasing and resealing of the device to take multiple transport measurements, it is possible the graphene is still damaged in the process or the shapes of the PI pores are altered in the tense state affecting transport measurement. Potentially a larger gasket and unexposed membrane area would distribute the force more equally, and thus less radial force would be applied to the membrane to stretch it. Also, a depression the size of the membrane in the bottom piece of the apparatus could be introduced to reduce the variability in pressure applied to the membrane. The membrane will be pressed the same amount each time the top disk is secured.

Future work could involve using another liquid besides water that is perhaps more volatile, but that graphene is still permeable to. A more volatile liquid like ethanol would have a larger vapor pressure, and likely a higher flow rate through the membrane. This would help to more easily assess changes in radiation performance if there is a larger absolute difference between graphene and no graphene in mass transport rate, given apparatus error stays below 5 %. Eventually, transport of hydrogen isotopes or helium will need to be tested. The apparatus/testing method would most likely have to change to measure the mass flow rate of these gases. However, this testing is essential in order to more accurately assess membrane performance in its specific fusion reactor role.

The irradiation of the graphene membranes using a gallium ion beam with 8 keV acceleration voltage and dosage of 2.53E+13 Gallium ions cm^{-2} did not significantly damage the graphene

membrane based off unchanging mass transport rates pre and post irradiation. This is promising since the graphene membrane is resilient to a significant dose of radiation damage that could be experienced in a fusion reactor. However, it is necessary to further investigate membrane performance at higher radiation dosages and bombardment energy to see at which dosage or bombardment energy a noticeable change in membrane performance will be observed. Additionally, correlating the radiation dosage from the gallium ions to an equivalent neutron dose that could be present in a fusion reactor setting is essential. Neutron damage to graphene can be assessed by using molecular dynamics and or physical radiation in an isotope reactor and subsequent Raman spectroscopy.[18,19] This can be related to ion irradiation by observing the level of damage in our samples in the SEM or potentially a spectrograph.

Imaging the graphene at higher resolutions could also be necessary in the future. Perhaps the majority of the present defects are on the nanoscale and are unobservable at the resolution of the current FIB/SEM system used. A higher resolution image could show if many nanotears are present and give a better sense for the graphene coverage on the sample and how this correlates with a transport measurement result. Also designing the top gasket such that contact could be made between the copper pin and the graphene sample would be essential. This would allow images of the graphene surface and nanopores to be taken immediately after irradiation of the sample to assess graphene coverage. This was not an issue when imaging the sample pre-irradiation, but is important to be able to see if the radiation damage can be observed in the SEM.

This is the first step in assessing how gas transport in 2D nanomaterials like graphene change under radiation conditions. Once, an accurate dosage of radiation that leads to a distinguishable change in graphene membrane performance is calculated, work can move towards assessing membrane performance at conditions expected in ARC and membrane performance over longer periods of time. Eventually, work will shift towards measuring gas transport of hydrogen isotopes across Pd based membranes when subjected to irradiation conditions expected in ARC.

6. REFERENCES

1. Smith, C. L.; Cowley, S. The Path to Fusion Power. *Philosophical Transactions of the Royal Society A: Mathematical, Physical and Engineering Sciences* **2010**, *368* (1914), 1091–1108.
2. Entler, S.; Horacek, J. Approximation of the Economy of Fusion Energy. *Energy* **2018**, *152*, 489–497.
3. Kovari, M., Coleman, M., Cristescu, I. & Smith, R. Tritium resources available for fusion reactors. *Nucl. Fusion* (2018). doi:10.1088/1741-4326/aa9d25
4. Segantin, S., Testoni, R. & Zucchetti, M. The lifetime determination of ARC reactor as a load-following plant in the energy framework. *Energy Policy* (2019). doi:10.1016/j.enpol.2018.11.010
5. Dingwall, S.; Mills, C. Human Health and the Biological Effects of Tritium in Drinking Water: Prudent Policy through Science – Addressing the ODWAC New Recommendation. *Dose-Response* **2011**, *9* (1).
6. Adhikari, S. & Fernando, S. Hydrogen membrane separation techniques. *Ind. Eng. Chem. Res.* **45,** 875–881 (2006).
7. Li, L. H.; Chen, Y. Atomically Thin Boron Nitride: Unique Properties and Applications. *Advanced Functional Materials* **2016**, *26* (16), 2594–2608.
8. Nine, M. J.; Cole, M. A. Graphene: a Multipurpose Material for Protective Coatings. *Journal of Materials Chemistry A* **2015**, *3* (24), 12580–12602.
9. O'Hern, S. C. *et al.* Selective ionic transport through tunable subnanometer pores in single-layer graphene membranes. *Nano Lett.* (2014). doi:10.1021/nl404118f
10. Suk, M. E.; Aluru, N. R. Water Transport through Ultrathin Graphene. *The Journal of Physical Chemistry Letters* **2010**, *1* (10), 1590–1594.
11. Kim, H. W.; Yoon, H. W. Selective Gas Transport Through Few-Layered Graphene and Graphene Oxide Membranes. *Science* **2013**, *342* (6154), 91–95.
12. Drahushuk, L. W.; Strano, M. S. Mechanisms of Gas Permeation through Single Layer Graphene Membranes. *Langmuir* **2012**, *28* (48), 16671–16678.
13. Huang, S.; Dakhchoune, M. Single-Layer Graphene Membranes by Crack-Free Transfer for Gas Mixture Separation. *Nature Communications* **2018**, *9* (1).
14. Kotakoski, J.; Krasheninnikov, A. V. Chapter 11. Native and Irradiation-Induced Defects in Graphene: What Can We Learn from Atomistic Simulations? *Theoretical and Computational Chemistry Series Computational Nanoscience* **2011**, 334–376.
15. OpenStaxCollege. https://opentextbc.ca/physicstestbook2/chapter/viscosity-and-laminar-flow-poiseuilles-law/ (accessed Jan 16, 2020).
16. Libretexts. Clausius-Clapeyron Equation https://chem.libretexts.org/Bookshelves/Physical_and_Theoretical_Chemistry_Textbook_Maps/Supplemental_Modules_(Physical_and_Theoretical_Chemistry)/Physical_Properties_of_Matter/States_of_Matter/Phase_Transitions/Clausius-Clapeyron_Equation (accessed Jan 16, 2020).
17. Tian, W.; Li, W. A Review on Lattice Defects in Graphene: Types, Generation, Effects and Regulation. *Micromachines* **2017**, *8* (5), 163.
18. Kryworuk, C.; The Effects of Neutron and Gamma Irradiation on Graphene; Mechanical Engineering, Virginia Polytechnic Institute **2013**
19. Huang, H.; Tang, X. Graphene Damage Effects on Radiation-Resistance and Configuration of Copper–Graphene Nanocomposite under Irradiation: A Molecular Dynamics Study. *Scientific Reports* **2016**, *6* (1).